EGYPTIAN JOURNAL OF BASIC AND APPLIED SCIENCES 3 (2016) 44–60

HOSTED BY

ELSEVIER

Available online at www.sciencedirect.com

ScienceDirect

journal homepage: http://ees.elsevier.com/ejbas/default.asp

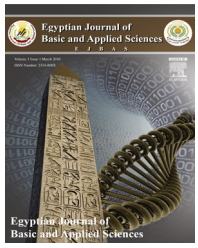

Full Length Article

Characterization, quantum, antibacterial, antifungal and antioxidant studies on Hg(II) and Cd(II) complexes of allyl and ethyl thiosemicarbazides derived from 2-aminothiazole-4-yl acetohydrazide

T.A. Yousef [a,b], *G.M. Abu El-Reash* [c,*], *O.A. El-Gammal* [c], *B.M. Sharaa* [a]

[a] *Department of Toxic and Narcotic Drug, Forensic Medicine, Mansoura Laboratory, Medicolegal Organization, Ministry of Justice, Egypt*

[b] *Department of Chemistry, Science College, Al Imam Mohammad Bin Saud Islamic University, (IMSIU), P.O Box 90950, Riyadh 11623, Saudi Arabia*

[c] *Department of Chemistry, Faculty of Science, Mansoura University, P.O. Box 70, Mansoura, Egypt*

ARTICLE INFO

Article history:
Received 26 May 2015
Received in revised form 16 August 2015
Accepted 2 September 2015
Available online 22 December 2015

Keywords:
Thiosemicarbazide complex
Spectral characterization
Thermal degradation
Biological activity

ABSTRACT

Two thiosemicarbazide ligands were derived from the addition of 2-(2-aminothiazol-4-yl) acetohydrazide to both ethyl isothiocyanate (H_2TAET) and allyl isothiocyanate (H_2TAAT) where their Cd (II) and Hg (II) complexes were synthesized and characterized by traditional techniques. The complexes were assigned the formulas $[Cd(HTAET)(H_2O)Cl](H_2O)_2$, $[Hg(TAET)(H_2O)_2]_2$, $[Cd(HTAAT)(H_2O)Cl]H_2O$ and $[Hg(H_2TAAT)(H_2O)Cl_2]$, respectively. In Cd (II) complexes, the IR spectra show that the ligands behave as monobasic bidentate through (C═N) thiazole ring and deprotonated enolized (CO). In Hg (II) complexes, H_2TAET acts as dibasic tridentate (NSO) via thiol (CS), enolized (CO) and new azomethine (N═C)* groups, while H_2TAAT acts as neutral tridentate (NNO) through (C═N) of thiazole ring, (CO) and new (C═N) due to SH formation. A tetrahedral geometry for Cd (II) complexes, square pyramidal geometry for $[Hg(TAET)(H_2O)_2]_2$ and octahedral geometry for $[Hg(H_2TAAT)(H_2O)Cl_2]$ were proposed. The data of theoretical and experimental vibrational frequencies of ligands are comparable. The calculated HOMO-LUMO energies gap data decided the possibility of charge transfer within the molecule. The binding energies calculations showed that the stability of complexes is higher than that of ligands. The kinetic and thermodynamic parameters of the Cd (II) complexes have been calculated by Coats–Redfern and Horowitz–Metzger methods. Moreover, the antimicrobial activities of the compounds have been discussed using a wide spectrum of bacterial and fungal strains. Representatives of the synthesized compounds were tested and evaluated for anti-oxidant and antitumour activities.

* *Corresponding author.* Tel.: +20 002 01000373155.
E-mail address: gaelreash@mans.edu.eg (G.M. Abu El-Reash).

http://dx.doi.org/10.1016/j.ejbas.2015.09.005

1. Introduction

Thiazole and its derivatives have shown a wide range of biological significance, for example vitamin B1 and the coenzyme cocarboxylase with a thiazole ring [1]. It is known that 2-aminothiazole is an effective compound with a broad range of biological activity; also, it is an intermediate in the preparation of antibiotics and dyes [2] according to more than one type of donor atoms in thiosemicarbazide derivatives and their pronounced microbial activities [3–5]. Their metal complexes have attracted considerable attention which can introduce novel reactivity and frequently stabilize the metal cluster framework [6–9]. As an extension of our study on thiosemicarbazide moiety [10–13], we report herein the preparation of Cd (II) and Hg (II) complexes derived from a new thiosemicarbazide, namely 2-amino-4-yl acetothiosemicarbazide ending by ethyl (H_2TAET) and allyl (H_2TAAT) groups. The study determined the structure of ligands and complexes by traditional techniques and conceded by molecular modelling, DFT calculations and their thermal degradation kinetics using Coats–Redfern and Horowitz–Metzger techniques. Also, the microbial activities of the prepared compounds have been studied using a wide spectrum of bacterial and fungal strains.

2. Experimental

2.1. Instrumentation and materials

All the chemicals used were from Aldrich and Fluka without further purification. Elemental analyses (C, H, N) have been determined with a Perkin-Elmer 2400 series II analyzer. The Molar conductance values (10^{-3} mol L^{-1}) of the complexes in DMF were measured using a Tacussel conductivity bridge model CD6NG. The IR spectra were shown at a Mattson 5000 FTIR spectrophotometer with KBr discs within the range of IR spectra 4000–400 cm^{-1}. Electronic spectra have been recorded on a Unicam UV–Vis spectrophotometer UV2. ^{1}H NMR and ^{13}C NMR were measured in d6-DMSO at room temperature on Bruker Bio Spin GmbH 400 MHz spectrometer. Thermogravimetric measurements (TGA, DTG and 20–800 °C) have been recorded on a DTG-50 Shimadzu thermo gravimetric analyzer with a heating rate of 10 °C/min and nitrogen flow rate of 15 ml/min.

2.2. Synthesis of H_2TAET and H_2TAAT

H_2TAET and H_2TAAT have been synthesized by heating 1 mmol of 2-(2-aminothiazol-4-yl) acetohydrazide with 1 mmol ethyl and allyl isothiocyanate under reflux for 2 h. The resulting precipitate that formed for each has been filtered, washed more than once with ethanol and dried under vacuum over anhydrous $CaCl_2$.

2.3. Synthesis of complexes

2.3.1. Preparation of Cd(II) and Hg(II) complexes

Dissolved Cd and Hg chloride (1.0 mmol) has been added to ethanolic solution of H_2TAET (0.259 g, 1.0 mmol) and H_2TAAT (0.271 g, 1.0 mmol). The mixture was refluxed for 2–3 h and the precipitates formed were filtered, washed and dried in a vacuum desiccator over anhydrous $CaCl_2$. The complexes are stable in air and insoluble in most organic solvents but soluble in both dimethyl formamide (DMF) and dimethyl sulphoxide (DMSO). The molar conductivity values of all complexes were determined in DMF at the range 1–18 $ohm^{-1}\,cm^2\,mol^{-1}$ of non-electrolytes. Unfortunately, we could not get single crystals from the solid metal complexes.

2.4. Biology

2.4.1. Antibacterial activity

Chemical compounds have been tested against gram positive *Staphylococcus aureus* and gram negative *Escherichia coli* bacteria. Each of the compounds dissolved in DMSO, this solution with concentration (1 mg /ml) were made ready by separately paper discs of Whatman filter paper which were prepared with standard size (5 cm) and cut with sterilized in an autoclave. The paper discs were soaked in the desired concentration of the complex solution and put in the Petri dishes containing nutrient agar media (agar 20 g + beef extract 3 g + peptone 5 g) seeded with *S. aureus* and *E. coli*. The Petri dishes have been incubated at 36 °C and the inhibition zones were recorded after 24 h of incubation. Each treatment was done three times. The antimicrobial activity of a standard antibiotic ampicillin was also recorded using the same concentration and solvents. The % activity index for the complex was determined by the following formula:

$$\%\text{Activity Index} = \frac{\text{Zone of inhibition by test compound (diametre)}}{\text{Zone of inhibition by standard (diametre)}} \times 100$$

2.4.2. Antifungal activity

Antifungal activity, depend on the growth inhibition rates of the mycelia of *Candida albicans* in Potato Dextrose Broth medium (PDB) to determine growth inhibition rates. It was detected from the infected organs on potato dextrose agar (potato 250 g + dextrose 20 g + agar 20 g) medium of the host plants. The cultures of the fungi were filtered by single spore isolation technique. The solution with the concentration 1 mg/ml for all compounds in DMSO has been synthesized for testing against spore germination. A drop of the solution of each concentration was kept separately on glass slides. The conidia and fungal reproducing spores hoisted up with the help of an inoculating needle, which mixed in every drop for all compounds separately. Each treatment was repeated three times and a parallel DMSO solvent control set was done concurrently on separate glass slides. All the slides have been incubated in humid chambers at 25 ± 2 °C for 24 h. Each slide was observed under the microscope for spore germination and finally per cent germination was determined. A zone of inhibition of growth referred to an indication of antifungal activity. The results have been also compared with a blank antifungal drug Clotrimazole at the same concentration.

2.4.3. Antioxidant activity

The antioxidant activity [14] employed a technique depending on measuring the reducing of stable free radicals. The

methodology explains that the consumption of the stable free radical (X') will be calculated by reactions as follows:

$$X' + YH \rightarrow XH + Y'$$

The rate or the extent of the process measured in terms of the decrease in X' concentration would be related to the ability of the added compounds to trap free radicals. The colour intensity of the solution will decrease due to scavenging of the free radical by the antioxidant material and this can be measured colorimetry at a specific wavelength. The assay employs the radical cation derived from 2,2′-azino-bis(3-ethylbenzthiazoline-6-sulphonic acid) (ABTS) or diphenyl picryl hydrazyl (DPPH) as stable free radical to be antioxidant and extracts. Inhibition per cent of free radical DPPH or ABTS has been determined owing to the equation:

$$I\% = (A_{blank} - A_{sample})/(A_{blank}) \times 100$$

where A_{blank} is the absorbance of the control reaction (containing all reagents except the test compound), and A_{sample} is the absorbance of the test sample.

2.4.3.1. *DPPH free radical activity*. All different concentrations of the tested chemical compounds under study have been dissolved in methanol to obtain final concentration ranging from 6.25 to 200 mg/ml to show IC_{50} (concentration makes 50% inhibition of DPPH colour). Fifty microlitres of different sample concentrations was added to 5 ml of 0.004% methanolic solution of DPPH. We let the solution dry for 60 min in the dark then the absorbance was recorded vs a blank at 517 nm.

2.4.3.2. *ABTS free radical activity*. For 3 ml of MnO2 solution (25 mg/ml), we added the solution containing both the investigated compounds and 2 ml of ABTS solution (60 mM). All were synthesized in 5 ml aqueous phosphate buffer solution (pH 7, 0.1 M). The solution was shaken, centrifuged, filtered and the absorbance of the resulting green–blue solution (ABTS radical solution) at λ734 nm was referred to approx. 0.5. Then, 50 ml of (2 mM) mixture of the tested compound in spectroscopic grade MeOH/phosphate buffer (1:1) was added. The absorbance was calculated, and the reduction in colour intensity was referred to inhibition percentage. L-ascorbic acid was used as a blank antioxidant (positive control). Blank was run without ABTS and using MeOH/phosphate buffer (1:1) instead of tested compounds.

Negative control was run with ABTS and MeOH/phosphate buffer (1:1) only [15,16].

2.4.4. In vitro *cytotoxic activities (MTT-dye reduction assay)*

In vitro cytotoxicity was done at a range of concentrations 500, 200, 100, 50, 10 and 1 μg/ml against mammary gland (Breast) MCF7 with a standard MTT assay as shown by Mosmann [17] with minor modifications [18]. The cell line made from ATCC through holding company for biological products and vaccines, Cairo, Egypt and cultured in RPMI 1640 medium with 10% foetal bovine serum. Antibiotics added were 100 units/ml penicillin and 100 μg/ml streptomycin at 37 °C in a 5% CO2 incubator. The reagents RPMI-1640 medium, MTT and DMSO and 5-fluorouracil (Sigma Co., St. Louis, MO, USA), Foetal Bovine serum (GIBCO, UK) and the cell line MCF7 (obtained from ATCC) have been used. MTT was based on the reduction of the yellow tetrazolium dye MTT to a violet formazan product through the mitochondrial succinate dehydrogenase in viable cells. MTT was poured at 5 mg/ml in PBS and filtered to remove a small amount of insoluble residue in some batches of MTT. The cells harvested from exponential phase have been plated in 96-well plates (104 cells/well in 100 μl of medium) and incubated for 24 h for attachment. Test compounds have been synthesized prior to the experiment by dissolving in 0.1% DMSO and diluting with medium. Considering the cytotoxicity effect of DMSO, the concentration of DMSO in the medium was set below 1%; under this condition, DMSO did not affect the growth and viability of the cell [19].

The cells have been then exposed to various concentrations of the compounds in the volume of 100 μl/well. Control wells have been synthesized by addition of an equal volume of the culture medium having 0.1% DMSO. Wells having culture medium without cells have been used as standard. 5-Fluorouracil was used as a blank anticancer drug for comparison. After 24 h, the medium was rinsed and cell cultures have been incubated by 100 μl MTT reagent (5 mg/ml MTT stock in PBS diluted to 1 mg/ml with 10% RPMI-1640 medium) for 4 h at 37 °C. The formazan produced by the viable cells was solubilized by using 100 μl DMSO. Then, the absorbances have been calculated at 570 nm using a plate reader (EXL 800) and the cytotoxic midpoint value, the concentration of chemical agent needed to reduce the spectrophotometric absorbance to 50% (IC_{50}), was shown by linear

Table 1 – Analytical and physical data of H_2TAET, H_2TAAT and their Cd(II) and Hg(II) complexes.

Compound molecular formula	(F.Wt)	Colour	M.P. (°C)	Found (calcd.)%					Yield %
				M	Cl	C	H	N	
H_2TAET	259.35	White	195	–	–	36.98	5.25	27.14	88
$C_8H_{13}N_5OS_2$						(37.05)	(5.05)	(27.00)	
$[Cd(HTAET)(H_2O)Cl](H_2O)_2$	460.24	Pale Yellow	202	24.72	6.16	20.85	3.91	15.21	91
$C_8H_{18}ClCdN_5O_4S_2$				(24.42)	(7.7)	(20.88)	(3.94)	(15.22)	
$[Hg(TAET)(H_2O)_2]_2$	987.9	Cream	210	40.37	–	19.63	3.16	14.28	92
$C_{16}H_{30}Hg_2N_{10}O_6S_{24}$				(40.61)		(19.45)	(3.06)	(14.18)	
H_2TAAT	271.36	White	165	–	–	39.96	4.66	26.03	85
$C_9H_{13}N_5OS_2$						(39.84)	(4.83)	(25.81)	
$[Cd(HTAAT)(H_2O)Cl]H_2O$	454.22	Yellowish white	222	24.77	7.64	23.78	3.34	15.65	93
$C_9H_{16}ClCdN_5O_3S_2$				(24.75)	(7.8)	(23.8)	(3.55)	(15.42)	
$[Hg(H_2TAAT)(H_2O)Cl_2]$	561.87	White	220	35.7	12.62	19.24	2.87	12.46	89
$C_9H_{15}Cl_2HgN_5O_2S_2$				(35.76)	(12.64)	(19.27)	(2.7)	(12.49)	

Table 2 – IR bands of H_2TAET, H_2TAAT and their Cd(II) and Hg(II) complexes.

Compound	ν(NH$_2$) found (Theo.)	ν(NH)[a] found (Theo.)	ν(NH)[b] found (Theo.)	ν(NH)[c] found (Theo.)	ν(C=O) found (Theo.)	ν(C=N)$_{th}$ found (Theo.)	ν(N=C)*	ν(C—O)	ν(N—N) found (Theo.)	ν/ δ (C=S) found (Theo.)	ν(C—S)	ν(SH)
H_2TAET	3360 (3496)	3282 (3359)	3146 (3486)	3107 (3496)	1680 (1607)	1641 (1607)	–	–	985 (956)	1323, 843 (1315), (828)	–	–
[Cd(HTAET)(H$_2$O)Cl](H$_2$O)$_2$	3378	–	–	3196	–	1622	1569	1223	1105	–	718	2337
[Hg(TAET)(H$_2$O)$_2$]$_2$	3413	–	–	3101	–	1626	1574	1197	1047	–	724	–
H_2TAAT	3437 (3515)	3342 (3462)	3278 (3462)	3179 (330)	1681 (1721)	1648 (1598)	–	–	982(996)	1330, 845 (1305),(866)	–	–
[Cd(HTAAT)(H$_2$O)Cl]H$_2$O	3398	–	–	3197	–	1622	1566	1197	1045	–	717	2360
[Hg(H$_2$TAAT)(H$_2$O)Cl$_2$]	3265	3182	–	3121	1695	1626	1537	–	1037	–	723	2358

Th, thiazole; Theo, theoretical.
* New.

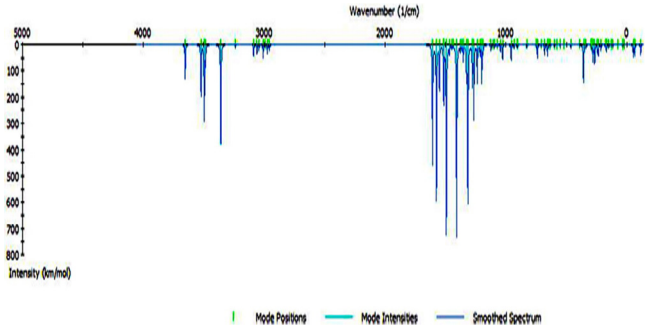

Fig. 1 – Theoretical IR spectrum of H_2TAET.

regression analysis with 95% of confidence limits. The IC_{50} was defined as the medium of two independent experiments through the equation of graphic line obtained. The experiment was performed in triplicate to get the mean values. The percentage viability was calculated using the formula

$$\text{The relative cell viability\%} = \frac{\text{A 570 of treated samples}}{\text{A 570 of untreated sample}} \times 100$$

2.5. *Molecular modelling*

We performed cluster calculations by DMOL^3 program [20] in Materials Studio program [21], which was designed for large scale density functional theory (DFT) calculations. DFT semi-core pseudo pods determinations (dspp) have been shown with the double numerical basis sets plus polarization (DNP) functional. The DNP basis sets are of comparable quality to 6-31G Gaussian basis sets [22]. Kessi and Delley assumed that the DNP basis sets are highly more accurate than Gaussian basis sets of the same size [23]. The RPBE functional [24] is so far the best exchange-correlation functional [25], based on the generalized gradient approximation (GGA), employed to take account of the exchange and correlation effects of electrons. The geometric optimization was shown without any symmetry restriction.

3. Results and discussion

The data of elemental analysis and some physical properties of the complexes were shown in Table 1.

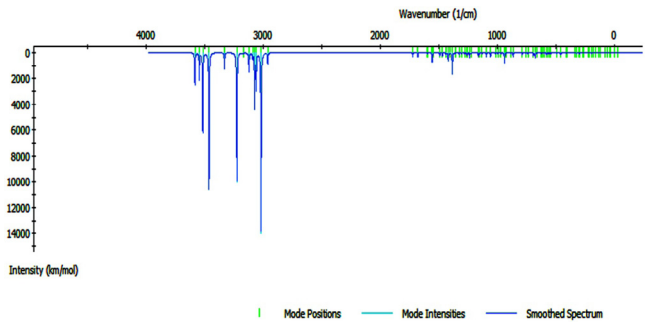

Fig. 2 – Theoretical IR spectrum of H_2TAAT.

3.1. *Molecular modelling*

3.1.1. *IR*

Theoretical calculations of the IR spectra of H_2TAET and H_2TAAT (Table 2) were carried out using a previously mentioned method (Figs. 1 and 2), and from a comparison with the experimental data we can conclude that: The calculated IR vibrations of H_2TAET and H_2TAAT show high agreement with the experimental data.

3.1.2. *Bond lengths and angles calculations*

The molecular structures along with atom numbering of H_2TAET, H_2TAAT and their complexes have been shown in Structures 1–6. Their analysis data and the calculated data of bond lengths and angles for the bonds are shown in Tables S1–S13 (Supplementary Materials), which give us the following concluding remarks:

i. All bond lengths of both ligands became slightly shorter in the complexes, except C(10)-S(16) which became slightly longer in $[Hg(H_2TAAT)(H_2O)Cl]_2$ [26].

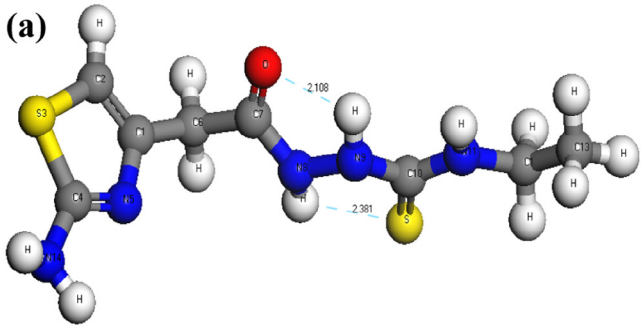

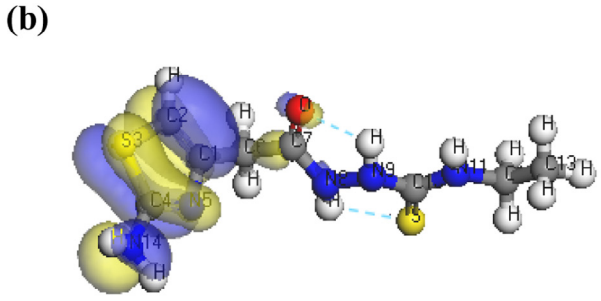

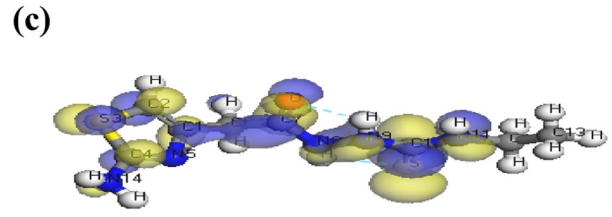

Structure 1 – Molecular structure of (a) H_2TAET, (b) HOMO of H_2TAET, (c) LUMO of H_2TAET.

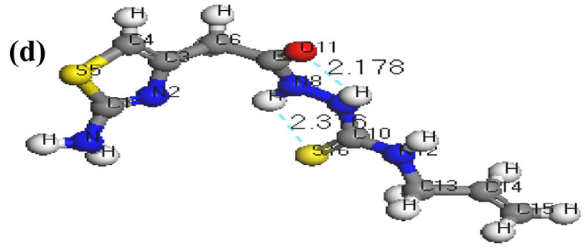

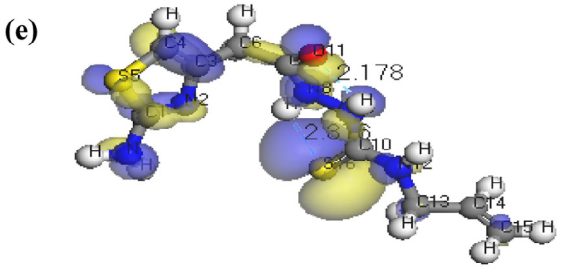

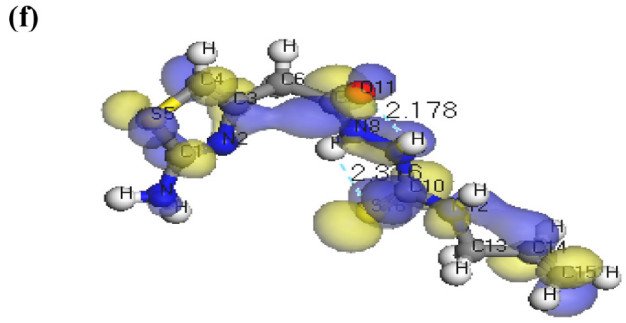

Structure 2 – Molecular structure of (d) H_2TAAT, (e) HOMO of H_2TAAT, (f) LUMO of H_2TAAT.

ii. In all Cd(II) and Hg(II) complexes, the bond distances [C(15)-N(7) and C(15)-O(16)] of H_2TAET and the bond distances [C(7)-N(8) and C(7)-O(11)] of H_2TAAT became shorter owing to the formation of M—O bond that makes C—O bond strong.

iii. In all complexes, the bond distances [C(1)-N(5) and N(5)-C(4)] of H_2TAET and the bond distances [C(1)-N(2) and N(2)-C(3)] of H_2TAAT are shorter. Due to formation of M—N bond in both Cd (II) and Hg(II) complexes of H_2TAAT, C—N bond weakened, which formed a double bond character.

iv. The bond angles of the thiosemicarbazide moiety of H_2TAET and H_2TAAT are altered somewhat upon coordination; the largest change affects C(1)-N(5)-C(3), O(16)-C(15)-N(7), N(8)-N(7)-C(15), C(9)-N(8)-N(7), N(8)-C(9)-S(13) and C(9)-N(10)-C(11) angles of H_2TAET and C(1)-N(2)-C(3), O(11)-C(7)-N(8), N(9)-N(8)-C(7), C(10)-N(9)-N(8), N(8)-C(10)-S(16) and C(10)-N(11)-C(12) angles of H_2TAAT which are reduced or increased on complex formation as a consequence of bonding.

v. The O(16)-C(15)-N(7) angle of H_2TAET changes from 119.92° to 118.74° in Cd complex owing to formation of

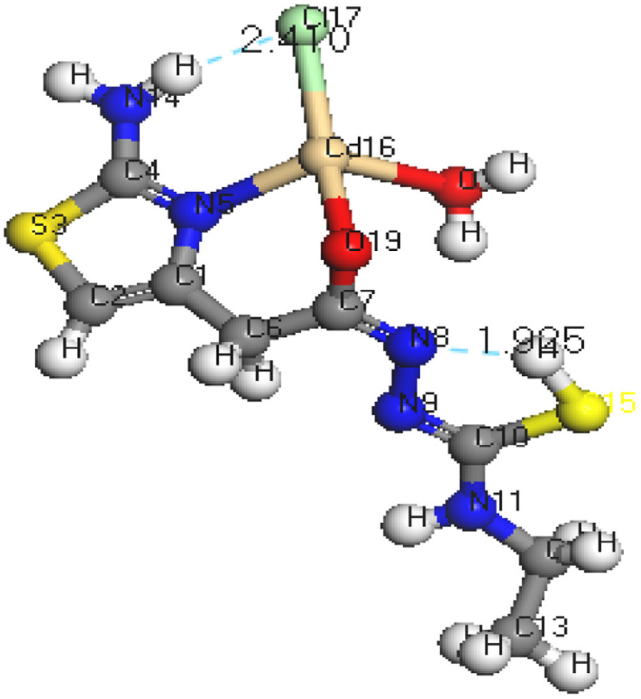

Structure 3 – Molecular structure of [Cd(HTAET)(H_2O)Cl](H_2O)$_2$.

O(19)-Cd(16)-N(5) chelate ring, whereas in H_2TAAT, the O(15)-C(7)-N(8) angle changes from 120.93° to 126.9° due to formation of O(15)-Cd(17)-N(3) chelate ring.

vi. The N(7)-N(8)-C(9) angle of H_2TAET changes from 119.81° to 119.82° and 119.33° in Hg complex owing to formation of S(16)-Hg(33)-N(8) and S(32)-Hg(38)-N(24), but in H_2TAAT, the N(9)-N(8)-C(7) angle changes from 112.46° to 120.504° owing to formation of N(9)-Hg(17)-O(15) and O(15)-Hg(17)-N(3) chelate angle.

vii. The bond angles N(5)-Cd(16)-O(19), O(19)-Cd(16)-O(18), O(18)-Cd(16)-Cl(17), Cl(17)-Cd(16)-N(5), and N(3)-Cd(17)-O(15), O(15)-Cd(17)-Cl(18), Cl(18)-Cd(17)-O(19), O(19)-Cd(17)-N(3) of Cd(II) complexes indicate that they are quite near to a tetrahedral geometry predicting sp^3 hybridization where Hg(II) of H_2TAET and H_2TAAT show a square pyramidal and adopt an octahedral arrangement predicting sp^3d^2 hybridization.

viii. The complexes were arranged by their $(M—N)_{azomethine}$ bond lengths as: Hg-N > Cd-N; reflecting Cd-N bond as the strongest among the others [27].

ix. The lower values of HOMO energy show that molecules donating electron ability are weaker. On the contrary, a higher energy of HOMO implies that it is a good electron donor. LUMO energy showed that the molecule can receive electron.

3.2. *IR spectral studies*

The most important IR frequencies have been shown in Table 2. The H_2TAET exhibits four bands at 3360, 3282, 3146 and 3107 cm^{-1} due to $\nu(NH_2)$, $\nu(NH)^a$, $\nu(NH)^b$ and $\nu(NH)^c$ respectively. While in H_2TAAT, $\nu(NH_2)$, $\nu(NH)^a$, $\nu(NH)^b$ and $\nu(NH)^c$ show

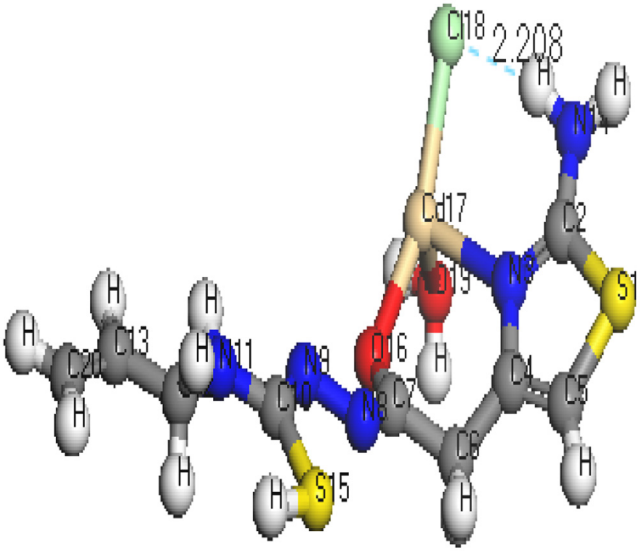

Structure 4 – Molecular structure of [Cd(HTAAT)(H_2O)Cl]H_2O.

bands at 3437, 3342, 3273 and 3179 cm^{-1}, respectively. The broadness of (NH) bands in both H_2TAAT and H_2TAET may be owing to the chance of H-bond formation as in Structures 1 and 2. The $\nu(C{=}N)_{th}$ of (H_2TAET and H_2TAAT) at 1641 and 1648 cm^{-1} undergoes a negative shift of wave number and the ν(C=N) thiazole ring appears at 1622 and 1626 cm^{-1} [28] in the Cd(II) and Hg(II).

Spectra of all complexes showed that the bands assigned to the newly formed (N=C)* band owing to the thiolating of the (C=S) group and enolization of (C=O) group were located at 1569 and 1574 cm^{-1} in the complexes of H_2TAET, respectively. While in complexes of H_2TAAT, the new (N=C)* band appears at 1566 and 1537 cm^{-1}, respectively. The bands

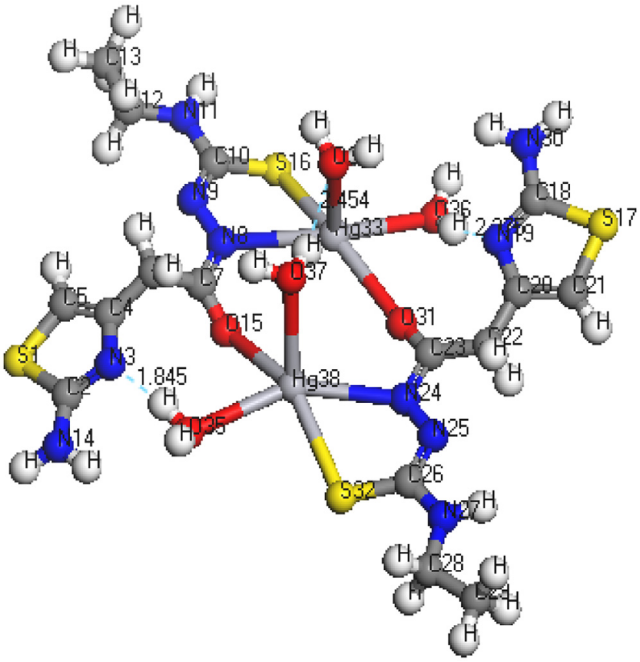

Structure 5 – Molecular structure of [Hg(HTAET)(H_2O)$_2$]$_2$.

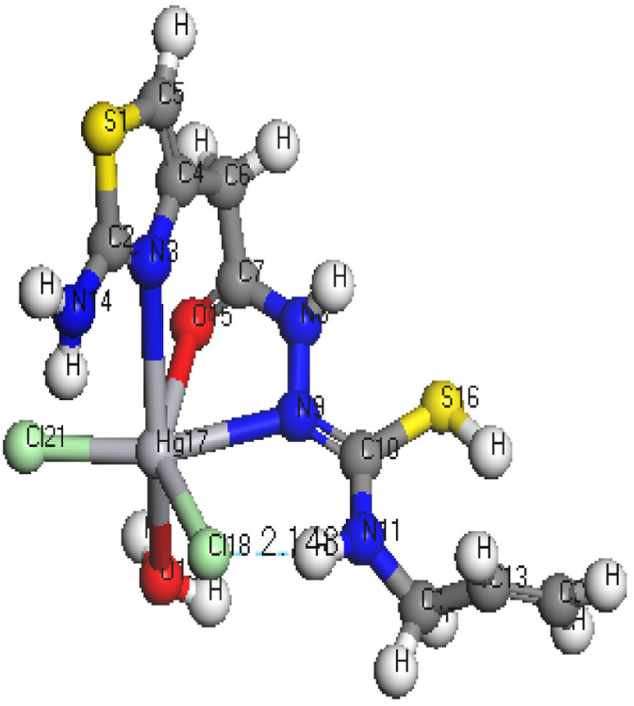

Structure 6 – Molecular sturcture of [Hg(H_2TAAT)(H_2O)Cl_2].

assigned to ν(C═O) in both ligands disappeared in both Cd(II) and Hg(II) complexes of H_2TAET with the appearance of an assigned band of ν(C—O) groups. On the other hand, the ν(C═O) in Hg(II) complex of H_2TAAT undergoes an increase in the band value resulting from the coordination to the metal. The strong bands observed at 985 and 982 cm^{-1} in both ligand spectra are assignable to the ν(N—N) vibrational modes. These bands were shifted to higher wave numbers in the complexes of H_2TAET, ν(C═S) and δ(C═S) appear at the frequencies 1323 and 843, while in H_2TAAT they appear at 1330 and 845 cm^{-1} [29]. In all complexes except in Hg(II) complex of H_2TAET, appearance of weak bands assigned to ν(C—S) owing to the formation of (SH) group without deprotonation. Based on the above evidence, the two ligands behave as monobasic bidentate through $(C{=}N)_{Th}$ and (C—O) groups in both Cd(II) complexes. In Hg(II) complexes, H_2TAET acts as dibasic tridentate via the sulphur atom of thiolate (C—S), oxygen atom of (C—O) and the new azomethine (N═C)* group. H_2TAAT acts as tridentate through $(C{=}N)_{Th}$, (C═O) and the new azomethine (N═C)* group. The positive shift of ν(N—N) is owing to the increase in the character of double bond of N—N showing the decrease of electron density through donation to metal ion and is a good evidence of coordination via azomethine nitrogen atom. In all complexes, appearance of bands in the regions 426–435 cm^{-1} and 464–531 cm^{-1} assigned to ν(M—N) and ν(M—O), respectively supports the proposed modes of coordination. Also, the spectra of complexes exhibit bands at ≈3389–3509, 873–860, and ≈565cm^{-1} referred to the coordinated water vibrations (Δ(H_2O), pr (H_2O) and Pw (H_2O), respectively.

3.3. ^{1}NMR studies

The ^{1}H NMR and ^{13}C spectra of H_2TAET, H_2TAAT and both complexes have been recorded in d_6-DMSO. The spectra of the H_2TAET (Fig. 3) revealing signals at δ 7.87, 9.23 and 9.9 ppm are assigned to $(NH)^a$, $(NH)^b$ and $(NH)^c$ respectively, which disappears on addition of D_2O. The signals at δ = 6.31, 6.89 and 3.3 ppm are attributed to CH of thiazole ring, (NH_2) and (CH_2) which are attached to the ring respectively. The signals owing to CH_2 protons of ethyl group appeared as a quartet at 3.48 ppm (q, J = 4, 2H) and those due to CH_3 protons as a triplet at 1.02 ppm (t, J = 6.96, 3H).

The ^{1}H NMR spectrum of the H_2TAAT represented in Fig. 4 shows signals at δ 8.10, 9.35 and 9.94 ppm are assigned to $(NH)^a$, $(NH)^b$ and $(NH)^c$ respectively, which disappears on addition of D_2O. The signals at δ = 3.31, 6.30 and 6.84 ppm are revealing to (CH_2) protons attached to the ring, (CH) group of thiazole ring and NH_2, respectively. The quartet signal at 4.36 ppm while the doublet at 5.03 ppm are assignable to the protons of CH_2 (—NH—CH_2) and CH_2 (—CH═CH_2), respectively. Moreover, the sextet signal centred at 5.78 ppm is assigned to the protons of the allyl CH group (ddd, J = 5.14, H).

In the ^{1}H NMR spectra of Cd(II) complexes and Hg(II) of H_2TAAT complexes (Figs. 5–7), the disappearance of the signal assignable to $(NH)^a$ and $(NH)^b$ protons and the appearance of SH proton at new signal at δ 10.18 and 10.21 ppm confirm the deprotonation of ligands without involving this S atom in

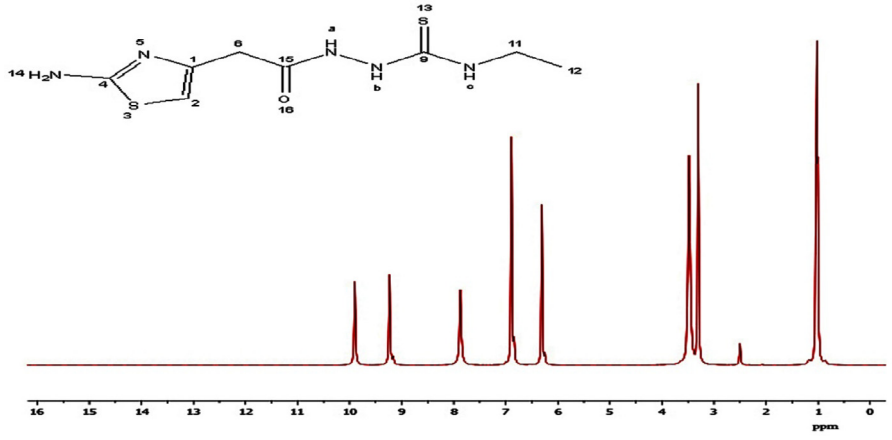

Fig. 3 – ^{1}H NMR spectrum of H_2TAET.

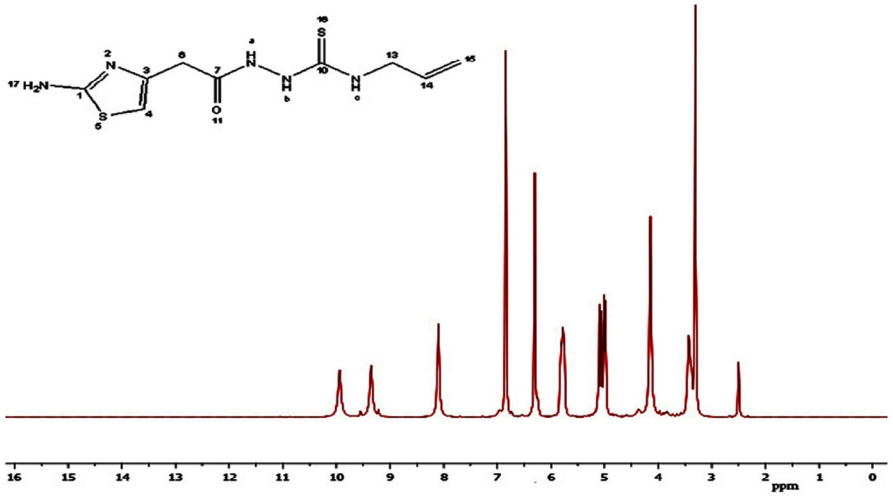

Fig. 4 – ^{1}H NMR spectrum of H_2TAAT.

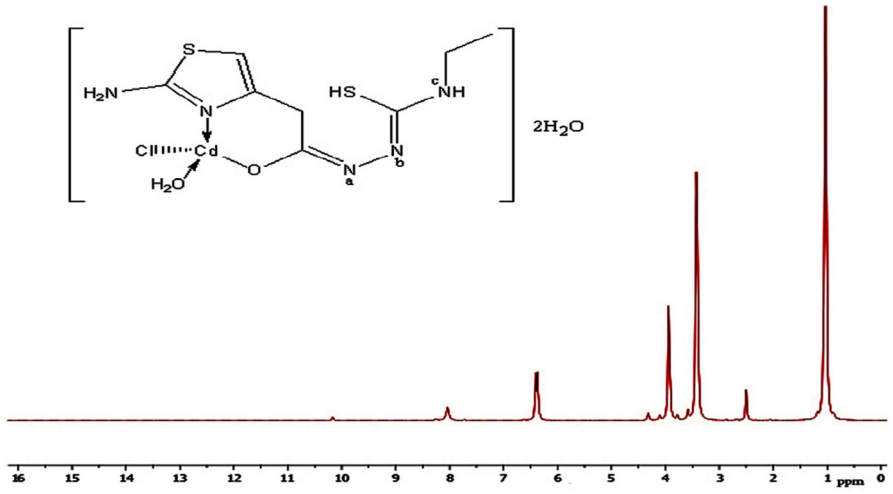

Fig. 5 – The ^{1}H NMR spectrum of $[Cd(HTAET)(H_2O)Cl](H_2O)_2$.

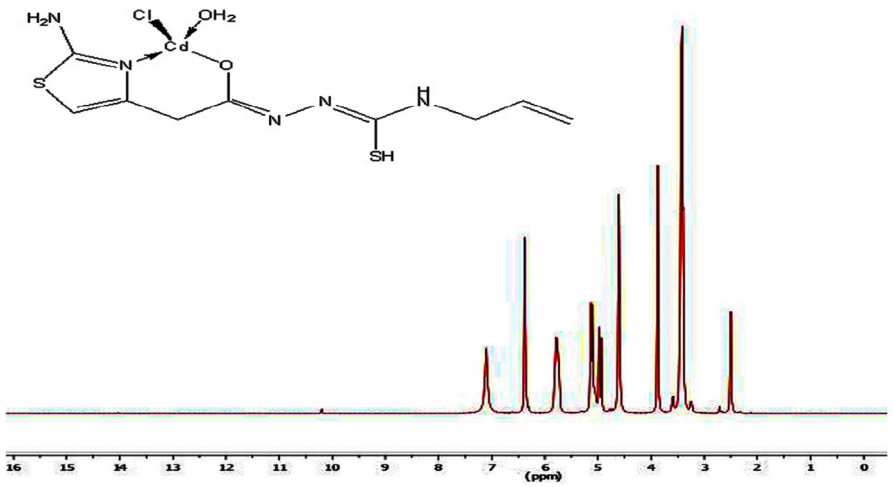

Fig. 6 – The ^{1}H NMR spectrum of $[Cd(H_2TAAT)(H_2O)Cl]H_2O$.

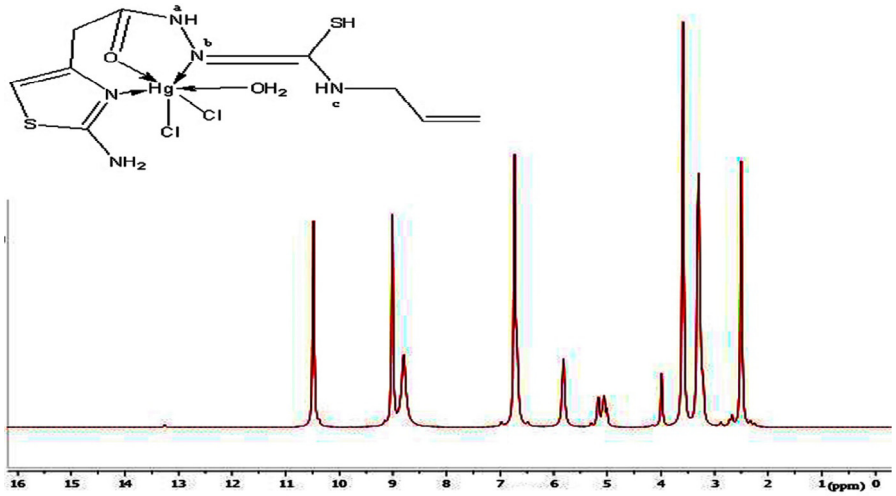

Fig. 7 – The ^{1}H NMR spectrum of [Hg(H_2TAAT)(H_2O)Cl_2].

coordination. But, in the ^{1}H NMR spectrum of Hg(II) complex of H_2TAET, the signal attributed to (NH)^{b} proton disappeared with the presence of signal at 10.49 due to SH group. Also, the shift of the signal owing to thiazole proton supports the coordination through (C═N)$_{Th}$. The conclusions drawn from this study lend further support to the mode of bonding discussed in IR spectra under study (Fig. 8).

The important peaks of ^{13}C NMR of ligands and its diamagnetic complexes are listed in Table 3. From the ^{13}C NMR data of the complexes, [Cd(HTAET)(H_2O)Cl](H_2O)$_2$ and [Cd(HTAAT)(H_2O)Cl]H_2O, the signals for the (C—SH), (C—N)$_{th}$, and (C—O) carbon led to an upfield shift compared to the corresponding free ligand. On other hand for [Hg(TAET)(H_2O)$_2$]$_2$ complex the signals for the (C—SH) carbon and (C—N)$_{th}$ carbon led to an up field shift compared to the free ligand. Finally for the complex [Hg(H_2TAAT)(H_2O)Cl_2] the signals for the (C—SH) carbon, (C—N)$_{th}$ carbon and (C—O) carbon showed an up field shift on complexation compared with the corresponding free ligand.

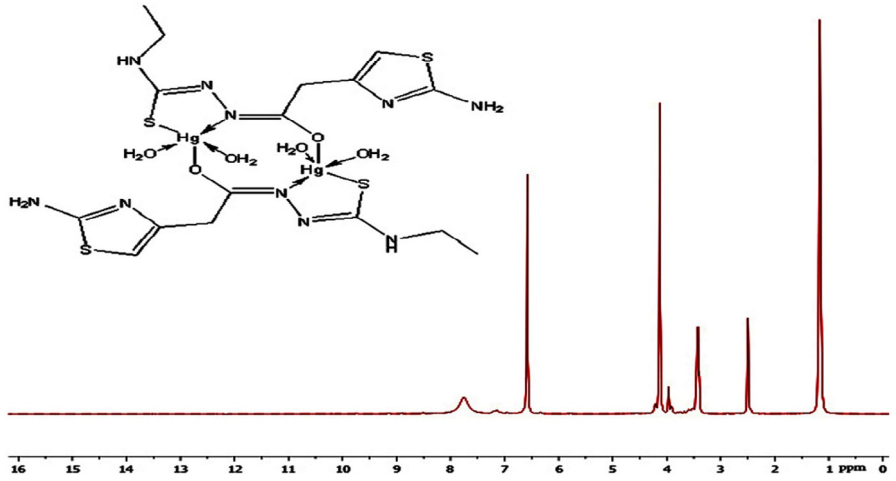

Fig. 8 – The ^{1}H NMR spectrum of [Hg(HTAET)(H_2O)$_2$]$_2$.

Table 3 – ^{13}C NMR chemical shifts in (ppm) assignments for H_2TAET, H_2TAAT and their Cd(II) and Hg(II) complexes.

Compound	C_1	C_2	C_4	C_6	C_9	C_{11}	C_{12}	C_{15}
H_2TAET	145.1	103.9	167.7	40.3	181.4	40.5	14.5	167.6
[Cd(HTAET)(H_2O)Cl](H_2O)$_2$	149.6	103.8	167.7	40.4	181.2	40.2	14.5	173.2
[Hg(TAET)(H_2O)$_2$]$_2$	149.9	103.9	167.8	40.5	181.3	40.4	14.3	174.1
Compound	C_1	C_3	C_4	C_6	C_7	C_{10}	C_{13}	C_{15}
H_2TAAT	166.7	145.8	103.6	40.6	166.3	183.0	47.0	116.4
[Cd(HTAAT)(H_2O)Cl]H_2O	166.8	149.9	103.5	40.5	172.8	183.1	47.2	116.4
[Hg(H_2TAAT)(H_2O)Cl_2]	166.9	145.9	103.8	40.3	173.5	188.8	47.1	116.5

Table 4 – Decomposition steps with the temperature range and weight loss for H_2TAET, H_2TAAT and their Cd(II) and Hg(II) complexes.

Compound	Temp. Range, °C	Removed species	Wt.Loss	
			Found%	Calcd%
$[Cd(HTAET)(H_2O)Cl](H_2O)_2$	62–89	$-2H_2O$	6.29	6.82
	113–134	$-H_2O$	3.49	3.92
	165–351	–Thiazole + NH_2	21.96	21.54
	391–556	$-C_2H_5Cl$	15.02	15.01
	695–745	$-H_2S + N_2 + NH_2 + C$	19.86	19.58
	745–800	$-CdO + C_2$ (residue)	33.57	33.12
	43–99.6	$-H_2O$	3.55	3.96
$[Cd(HTAAT)(H_2O)Cl]H_2O$	160–283	$-H_2O$	4.9	3.96
	313–362	$-H_2S + NH_2 + N_2 + CH_4$	20.54	20.69
	411–554	–HCl	8.45	8.03
	598–721	–Thiazole + NH_2	20.17	20.7
	725–800	–CdO + 5C (residue)	42.16	42.34

3.4. *Thermogravimetric studies*

Thermogravimetric analysis data (TGA) for Cd (II) complexes were shown in Table 4. One of the aims in the TGA data showed that the associated molecules of water within complexes support the elemental analyses. The data represented in Table 4 indicate that water of crystallization has been lost in temperature range 75–147 °C. Also, the TG thermograms for the same complexes represented a high part of residual including M—O with carbon revealing a good stability of the formed chelates.

3.5. *Kinetic data*

The influences of the structural properties of chelating agent on the thermal behaviour of complexes, the order (n) and the heat of activation E_a of the different decomposition stages have been determined from the TG and DTG by Coats–Redfern [30] (Figs. 9 and 10) and Horowitz–Metzger [31] (Figs. 11 and 12).

The $\left(\frac{d\alpha}{dt}\right)$ rate of thermal decomposition expressed by the Arrhenius equation has the following form:

Table 5 – Kinetic parameters of complexes evaluated by Coats–Redfern equation.

Compound	Peak	Mid Temp(K)	E_a KJ\mol	A (S^{-1})	ΔH^* KJ\mol	ΔS^* KJ\mol·K	ΔG^* KJ\mol
$[Cd(HTAET)(H_2O)Cl](H_2O)_2$	1st	352.32	112.02	13.97×10^{14}	109.09	0.033	97.4
	2nd	398.02	211.94	1.42×10^{26}	208.63	0.2533	107.78
	3rd	527.4	251.27	2.78×10^{27}	247.56	0.277	124.13
	4th	713.5	139.26	7.43×10^{4}	133.33	–0.101	205.72
	5th	990.24	673.65	2.11×10^{33}	665.42	0.38	286.09
$[Cd(HTAAT)(H_2O)Cl]H_2O$	1st	344.3	52.48	5.3×10^{4}	54.62	–0.11	95.01
	2nd	494.51	322.59	3.18×10^{40}	319.24	0.053	106.68
	3rd	610.23	236.37	1.37×10^{18}	231.3	0.096	172.48
	4th	755.43	96.14	1.2×10^{2}	89.86	–0.172	221.42
	5th	932.44	235.9	2.62×10^{10}	228.18	–0.055	279.41

Table 6 – Kinetic parameters of complexes evaluated by Horowitz–Metzger equation.

Compound	Peak	Mid Temp(K)	E_a KJ\mol	A (S^{-1})	ΔH^* KJ\mol	ΔS^* KJ\mol·K	ΔG^* KJ\mol
$[Cd(HTAET)(H_2O)Cl](H_2O)_2$	1st	352.32	116.37	1.68×10^{15}	113.44	0.045	97.53
	2nd	398.02	219.51	5.28×10^{27}	216.2	0.2723	107.83
	3rd	527.4	252.95	4.26×10^{27}	249.24	0.231	124.22
	4th	713.5	150.00	4.34×10^{8}	144.07	–0.087	206.00
	5th	990.24	684.47	7.69×10^{33}	676.24	0.3914	286.36
$[Cd(HTAAT)(H_2O)Cl]H_2O$	1st	344.3	63.02	3.5×10^{6}	60.16	–0.102	95.16
	2nd	494.51	332.29	5.78×10^{41}	328.94	0.55	106.85
	3rd	610.23	246.18	9.23×10^{18}	241.1	0.11	172.61
	4th	755.43	108.3	8.7×10^{3}	102.41	–0.161	221.76
	5th	932.44	283.3	1.47×10^{13}	275.54	–0.0023	277.67

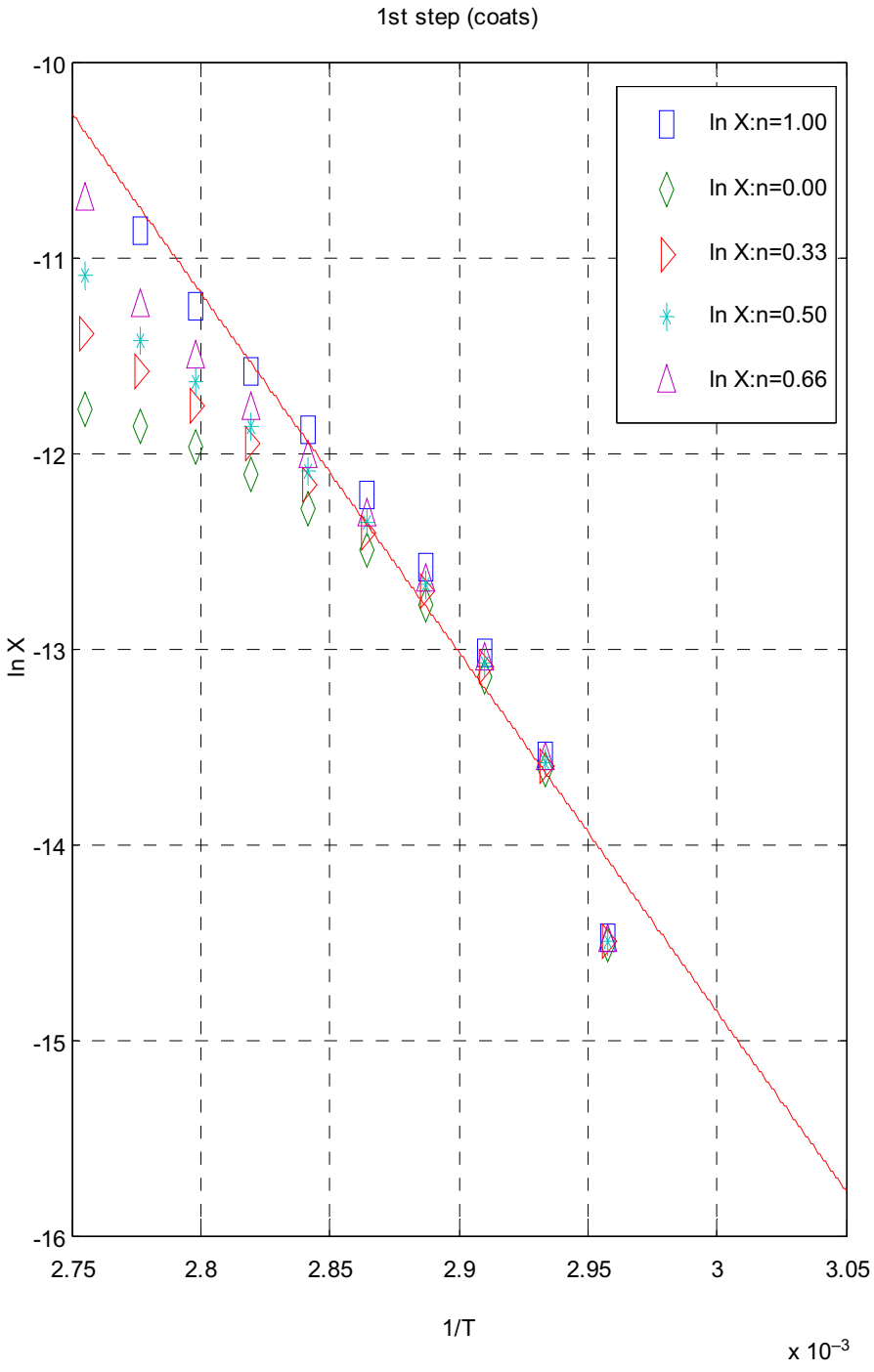

Fig. 9 – First step Coats–Redfern of $[Cd(HTAET)(H_2O)Cl](H_2O)_2$.

$$\frac{d\alpha}{dt} = A\exp\left(-\frac{E_a}{RT}\right)g(\alpha) \quad (1)$$

where (A) is the Arrhenius pre-exponential factor; (E_a) is the activation energy; (R) is the gas constant and g(α) is the differential conversion factor and equal (1-α)n where n is the reaction order, assumed to remain constant through the reaction. The degradation of metal complexes was shown as first order reaction. Under this assumption the integration of Equation (1) leads to:

$$\ln(1-\alpha) = -\frac{A}{\beta}\int_{T_o}^{T}\mathrm{Exp}\left(-\frac{E_a}{RT}\right)dT \quad (2)$$

From Equation (2), the degradation kinetic parameters A and E_a can be determined. Thermodynamic parameters can be

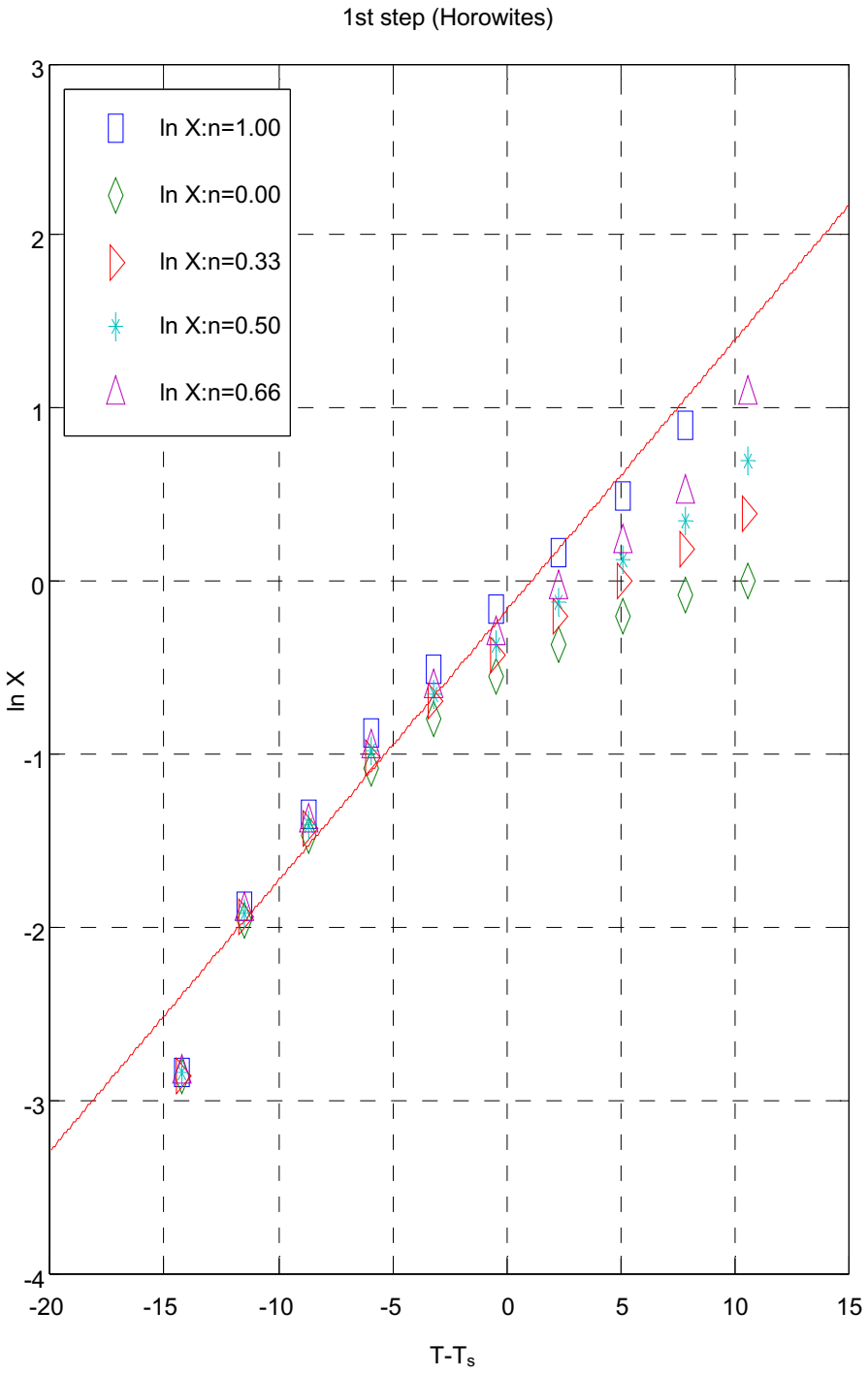

Fig. 10 – First step Coats–Redfern of $[Cd(H_2TAAT)(H_2O)Cl]H_2O$.

determined by the Eyring equation [32]. From results obtained in Tables 5 and 6, the following remarks showed that:

i. Decomposition steps showed a best fit of n = 1.
ii. A (+) sign of activation enthalpy, ΔH^* shows that the decomposition steps were endothermic processes.
iii. The activation energy Ea of complexes increases, indicating the higher stability of the remaining part due to their covalent bond character [33] and the decrease of E_a on going from $[Cd(HTAET)(H_2O)Cl](H_2O)_2$ complex to $[Cd(HTAAT)(H_2O)Cl](H_2O)$ complex reflects the greater thermal stability of the first one than the second complex as E_a depends on the strength of (O→M←N).
iv. The (+) sign of ΔG^* for the complexes reveals that all the decomposition stages were nonspontaneous processes.

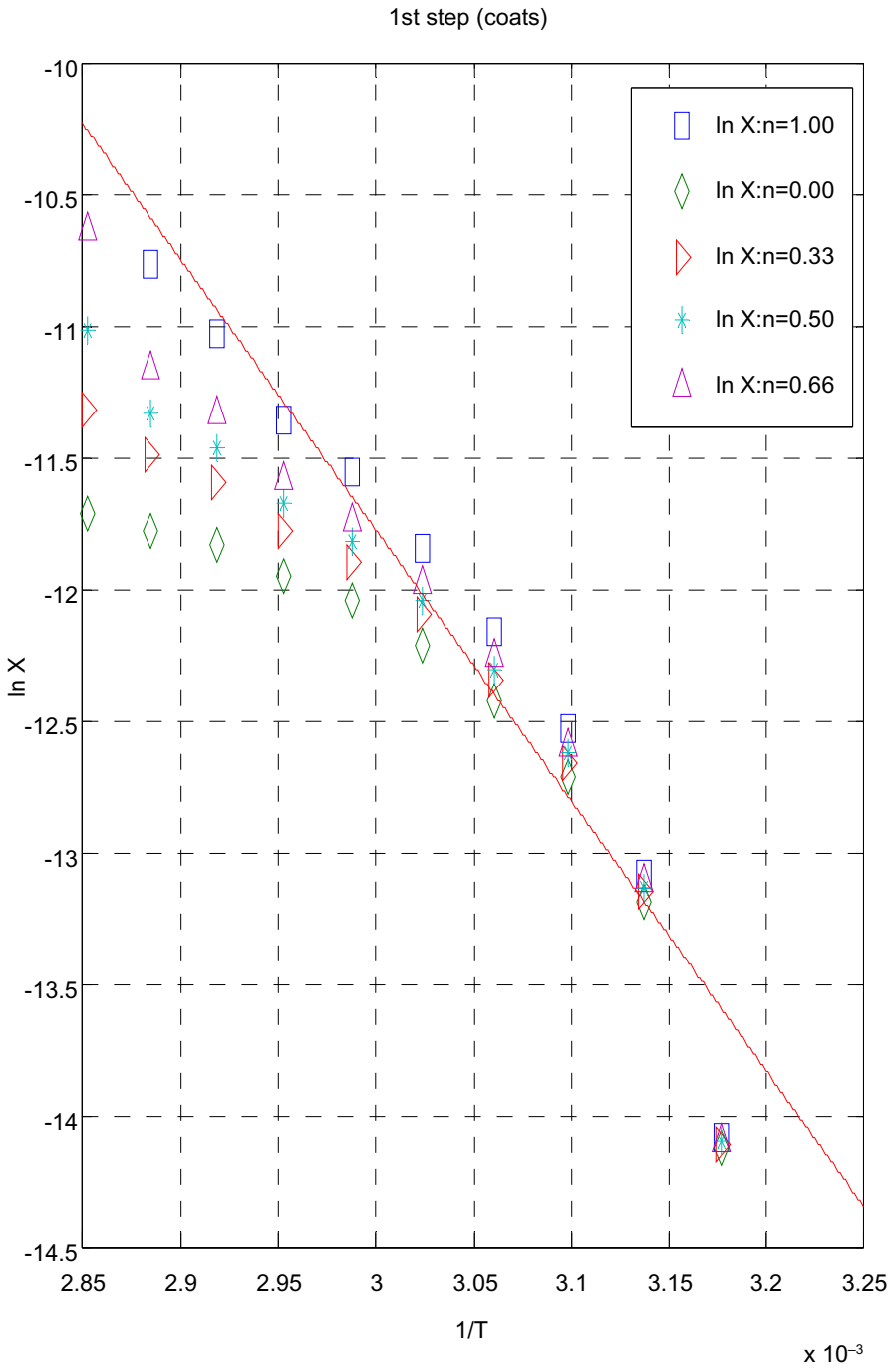

Fig. 11 – First step Horowitz–Metzger plots of $[Cd(HTAET)(H_2O)Cl](H_2O)_2$.

3.6. *Biological studies*

3.6.1. *Antifungal activity*

In our screening of antimicrobial activity it has been shown that the studies must lead to an overall comparison of activities between the H_2TAET, H_2TAAT and their complexes so that the mechanism of their activities can be understood. The experimental antifungal activity data (Table 7) indicate that H_2TAET, H_2TAAT and their complexes show an appreciable activity against *C. albicans*. DMSO control has shown a negligible activity as compared to H_2TAET, H_2TAAT and their complexes.

$[Hg(TAET)(H_2O)_2]_2$ showed a highly good activity (92.6%) compared with the rest of the complexes. From the data, we also observed that complexes are more active than the corresponding ligands. The toxicity of complexes was related to the strength of metal–ligand bond, besides other factors such as the size of the cation [34]. The action mode of the compounds may involve formation of a hydrogen bond via the azomethine group (>C═N—) with the active centres of cell constituents resulting in interferences with the normal cell process.

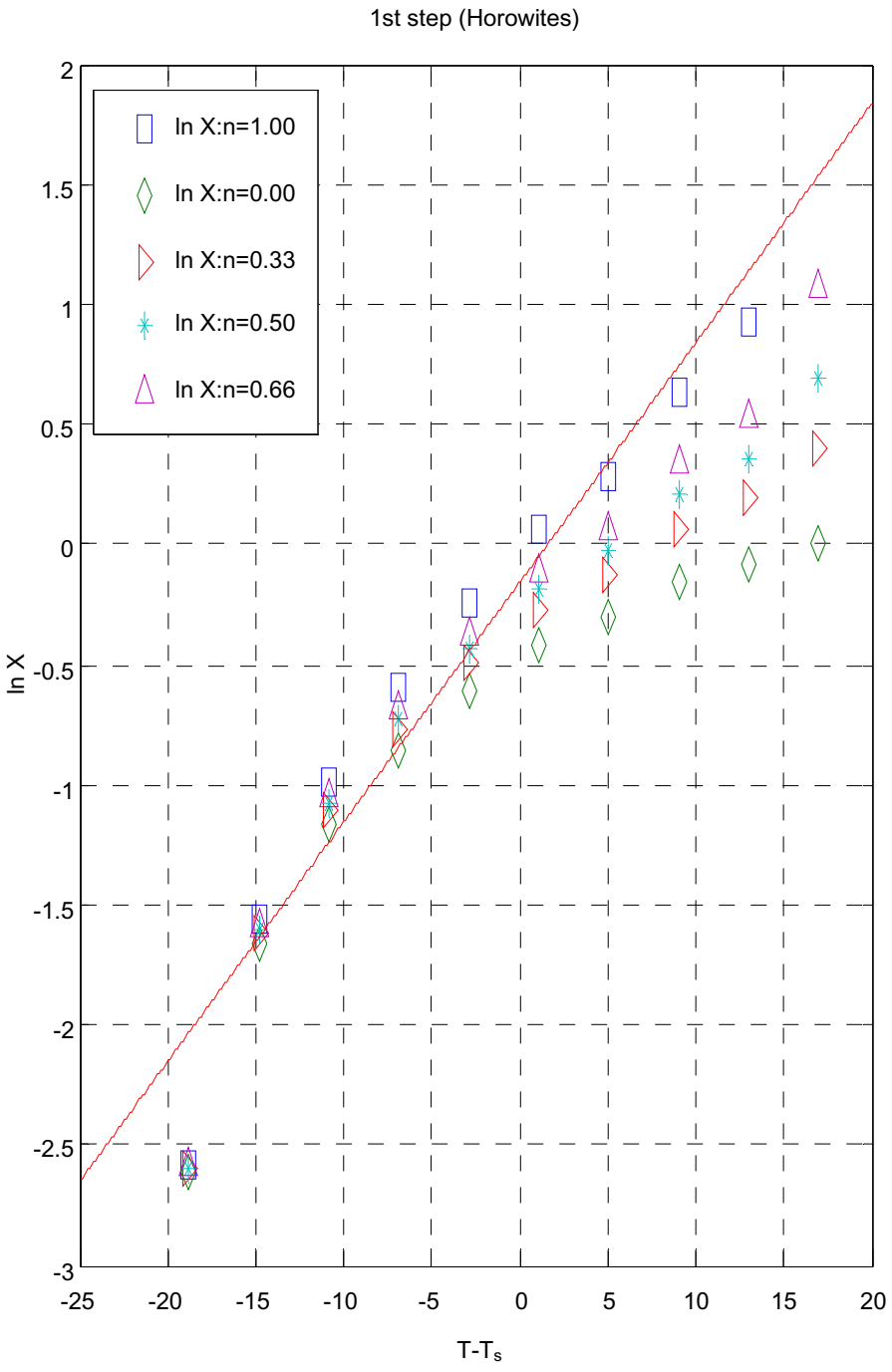

Fig. 12 – First step Horowitz–Metzger plots of [Cd(H_2TAAT)(H_2O)Cl]H_2O.

3.6.2. *Antibacterial activity*

H_2TAET, H_2TAAT and their complexes, standard drug Ampicillin and DMSO solvent were screened separately for their antibacterial activity vs *E. coli* and *S. aureus*. Activity of complexes has been compared to activity of a standard antibiotic Ampicillin and % Activity Index for the complexes has been calculated. The antibacterial results (Table 7) suggest that [Cd(HTAAT)(H_2O)Cl]H_2O, [Cd(HTAET)(H_2O)Cl](H_2O)$_2$ and [Hg(TAET)(H_2O)$_2$]$_2$ show highest activity against both bacteria [26,34] as compared to the standard drug. The complexes show higher antibacterial activity than their corresponding ligands.

The complexes with negative results showed inability of it to diffuse into the Gram-negative bacteria cell membranes and hence unable to interfere its biological activity and inactivated by unknown cellular mechanism i.e. bacterial enzymes.

The (+) results suggested the highest diffusion of complexes into the bacterial cells and this complexes with positive results are able to kill the bacterium as shown by the zones of inhibition of bacterial growth [34].

Table 7 – Antibacterial and antifungal activity of H_2TAET, H_2TAAT and their Cd(II) and Hg(II) complexes.

Compound	*E. coli* (mg/ml)		*S. aureus* (mg/ml)		*C. albicans* (mg/ml)	
	Diameter of inhibition zone (in mm)	% Activity index	Diameter of inhibition zone (in mm)	% Activity index	Diameter of inhibition zone (in mm)	% Activity index
H_2TAET	20	80	14	60.9	NA	–
$[Cd(HTAET)(H_2O)Cl](H_2O)_2$	25	100	23	100	22	81.5
$[Hg(TAET)(H_2O)_2]_2$	25	100	23	100	25	92.6
H_2TAAT	6	24	22	95.6	6	22.2
$[Cd(HTAAT)(H_2O)Cl]H_2O$	25	100	21	91.3	21	77.7
$[Hg(H_2TAAT)(H_2O)Cl_2]$	7	28	22	95.6	9	33.3
Ampicillin	25	100	23	100	NA	–
Clotrimazole	NA	–	NA	–	27	100

NA, No Activity.

3.6.3. *Antioxidant activity*

Increasing effect of the radical-scavenging of phenolic acids and their ester derivatives (Table 8) and the antioxidant capacity assays (DPPH 2- diphenyl-1-picrylhydrazyl radical; ABTS 2,2′-azino-bis(3-ethylbenzthiazoline-6-sulphonic acid) were used. The DPPH method was done in a homogeneous phase with the advantage of establishing a real ranking hierarchy of antioxidant activity of electron- or H-donating agents, where DPPH method was not affected by any factors and this leads to interfere with another model systems, as metal chelation or partitioning abilities [35,36]. The generation of the ABTS radical cation is a basis of other spectrophotometric methods that are currently being used for the calculations of antioxidant activity in solutions of pure substances, mixtures and beverages [37]. Where H2TAET, H2TAAT and $[Cd(HTAAT)(H_2O)Cl]H_2O$ showed the best activity which are near to standard Ascorbic acid comparing to the ABTS•+ radical-scavenging activity.

The data obtained with DPPH radical revealed that all compounds showed good antioxidant capacity except $[Cd(HTAET)(H_2O)Cl](H_2O)_2$ which showed low activity while $[Hg(TAET)(H_2O)_2]_2$ showed moderate activity, as shown in Table 8. The effective anticancer drug, "5-fluorouracil" has been used as standard.

3.6.4. In vitro *cytotoxic activities (MTT-dye reduction assay)*

In vitro cytotoxic tests were conducted utilizing all the prepared compounds against human tumour cell line MCF7 normal cell line by means of a colorimetric assay (MTT assay) that measures mitochondrial dehydrogenase activity as an indication of cell viability. The activities corresponding to viability of growth cell cancer are shown in Table 9. In parallel, the effectiveness of spread used anticancer drug, "5-fluorouracil" has been used as standard. H_2TAAT and its complexes covered a high range of activity with viability (%) near the standard. 5-Florouracil indicated that these compounds exhibited anti-tumour activity vs. cell lines without causing significant damage to normal cells. H_2TAET and its complexes showed low potential activity. It means that the chemical structure of compounds is important to express biological activity of the complex and can be essential in designing and synthesizing anti-cancer drugs.

4. Conclusion

The addition of 2-(2-amino thiazole -4-yl acetohydrazide) to both ethyl isothiocyanate (H_2TAET) and allyl isothiocyanate (H_2TAAT) has shown a versatility that leads to a rise in the complexes with metal chlorides by various stoichiometries in spite of similar experimental conditions. The experimental and theoretical frequency results of ligands are comparable. The calculated HOMO-LUMO energies gap confirmed the possibility of charge transfer. Also, the data of thermal degradation of the solid complexes were shown by Coats–Redfern and Horowitz–Metzger methods. $[Cd(HTAAT)(H_2O)Cl]H_2O$, $[Cd(HTAET)(H_2O)Cl](H_2O)_2$ and $[Hg(TAET)(H_2O)_2]_2$ showed high antibacterial activity while $[Hg(TAET)(H_2O)_2]_2$ showed the highest antifungal activity. The present results are of significance, considering the pharmacological and antimicrobial activity of thiosemicarbazides; therefore, compound $[Hg(TAET)(H_2O)_2]_2$ can be used as a promising antimicrobial activity agent.

Table 8 – Free radical scavenging capacities of H_2TAET, H_2TAAT and their Cd(II) and Hg(II) complexes measured in DPPH and ABTS assay.

Compound	DPPH inhibition (%)				Absorbance	ABTS inhibition (%)
Ascorbic acid	100 ppm	200 ppm	500 ppm	1000 ppm	0.019	96.57
H_2TAET	10.75	19.83	45.49	91.32	0.031	94.28
$[Cd(HTAET)(H_2O)Cl](H_2O)_2$	10.06	18.92	45.50	89.80	0.342	35.23
$[Hg(TAET)(H_2O)_2]_2$	5.91	9.67	19.95	35.75	0.114	78.66
H_2TAAT	9.25	15.31	33.49	63.79	0.029	94.28
$[Cd(HTAAT)(H_2O)Cl]H_2O$	10.32	18.91	43.80	86.03	0.042	91.42
$[Hg(H_2TAAT)(H_2O)Cl_2]$	8.65	17.09	42.41	84.61	0.150	71.80

Table 9 – MTT viability (percentage) assay of various concentrations of H_2TAET, H_2TAAT and their Cd(II) and Hg(II) complexes.

Compound	Conc.					
	MTT viability (%)					
	500 ppm	200 ppm	100 ppm	50 ppm	10 ppm	1 ppm
5-Florouracil	27.308	29.336	31.399	33.322	36.888	41.993
H_2TAET	63.769	60.007	62.874	65.727	71.825	85.965
$[Cd(HTAET)(H_2O)Cl](H_2O)_2$	58.091	62.098	63.636	65.434	63.790	74.475
$[Hg(TAET)(H_2O)_2]_2$	41.552	47.399	47.972	50.280	55.091	60.021
H_2TAAT	24.070	27.007	29.000	31.273	34.280	40.89
$[Cd(HTAAT)(H_2O)Cl]H_2O$	29.426	31.413	33.161	37.573	40.825	42.336
$[Hg(H_2TAAT)(H_2O)Cl_2]$	30.105	32.552	33.8112	35.699	39.301	42.972

Appendix: Supplementary material

Supplementary data associated with this article can be found in the online version at doi:10.1016/j.ejbas.2015.09.005.

REFERENCES

[1] Schrauzer GN, Kohnle J. Coenzym B12-modelle. Chem Ber 1964;97:3056–63.
[2] Dash B, Patra M, Praharaj S. Synthesis and biological-activity of some Schiff-bases derived from thiazoles and benzothiazoles. Indian J Chem 1980;19B:894–7.
[3] Ali Akbar M, Livingstone SE. Metal complexes of sulphur-nitrogen chelating agents. Coord Chem Rev 1974;13:101–32.
[4] Campbell MJM. Transition metal complexes of thiosemicarbazide and thiosemicarbazones. Coord Chem Rev 1975;15:279–319.
[5] Padhye S, Kauffman GB. An unusual dimeric structure of a Cu(I) Bis(thiosemicarbazone) complex: implications for the mechanism of hypoxic selectivity of the Cu(II) derivatives. Coord Chem Rev 1985;63:127–60.
[6] Au YK, Cheung K-K, Wong W-T. Synthesis and structural characterization of ruthenium and osmium carbonyl clusters containing 4, 6-dimethylpyrimidine-2-thione. Inorganica Chim Acta 1995;228:267–75.
[7] Au YK, Cheung K-K, Wong W-T. Synthesis, structural characterization and thermal reactivities of osmium carbonyl clusters containing 4, 6-dimethylpyrimidine-2-thione. J Chem Soc Dalton Trans 1995;1047–57.
[8] Deeming AJ, Hardcastle KI, Karim M. Suppression of cluster unsaturation by formation of extensive but long-range metal-metal bonding: crystal structures of $[Ru_3H(pyS)(CO)_9]$ and [{Ru3H(pyS)(CO)7}3], where pyS is the pyridine-2-thiolato ligand. Inorg Chem 1991;31:4792–6.
[9] Brodie AM, Holden HD, Lewis J, Taylor MJ. The reaction of $[Os_3(CO)_{10}(MeCN)_2]$, with heterocyclic thioamides. The crystal and molecular structure of $[Os_3(\mu\text{-}H)(CO)_{10}(\mu\text{-}SC$[double bond, length half m-dash]$NCH_2CH_2S)]$. J Chem Soc Dalton Trans 1986;633–9.
[10] Yousef TA, Badria FA, Ghazy SE, El-Gammal OA, Abu El-Reash GM. In vitro and in vivo antitumor activity of some synthesized 4-(2-pyridyl)-3-Thiosemicarbazides derivatives. J Med Med Sci 2011;3:37–46.
[11] Yousef TA, El-Gammal OA, Ghazy SE, Abu El-Reash GM. Synthesis, spectroscopic characterization, pH-metric and thermal behavior on Co (II) complexes formed with 4-(2-pyridyl)-3-thiosemicarbazide derivatives. J Mol Struct 2011;1004:271–83.
[12] El-Gammal OA, Abu El-Reash GM, Ghazy SE, Yousef TA. Heterocyclic substituted thiosemicarbazides and their Cu (II) complexes: synthesis, spectral characterization, thermal, molecular modeling, and DNA degradation studies. J Coord Chem 2012;6510:1655–71.
[13] Ghazy SE, Abu El-Reash GM, El-Gammal OA, Yousef TA. Flotation separation of mercury (II) from environmental water samples using thiosemicarbazide derivatives as chelating agents and oleic acid as surfactant. Chem Speciat Bioavail 2010;22:127–34.
[14] Aliage C, Lissi EA. Reaction of 2,2′-azinobis (3-ethylbenzothiazoline-6-sulfonic acid) (ABTS) derived radicals with hydroperoxides. Int J Chem Kinet 1998;30:565–70.
[15] Lissi E, Modak B, Torres R, Escobar J, Urza A. Total antioxidant potential of resinous exudates from Heliotropium species, and a comparison of the ABTS and DPPH methods. Free Radic Res 1999;30:471–7.
[16] Aeschlach R, Loliger J, Scott CB, Murcia A, Butler J, Halliwel B, et al. Antioxidant actions of thymol, carvacrol, 6-gingerol, zingerone and hydroxytyrosol. Food Chem Toxicol 1994;32:31–6.
[17] Mosmann T. Rapid colorimetric assay for cellular growth and survival: application to proliferation and cytotoxicity assays. J Immunol Methods 1983;65(1):55–63.
[18] Konstantinov SM, Eibl H, Berger MR. BCR-ABL influences the antileukaemic efficacy of alkylphosphocholines. Br J Haematol 1999;107(2):365–80.
[19] Dodoff N, Grancharov K, Gugova R, Spassovska N. Platinum (II) complexes of benzoic-and 3-methoxybenzoic acid hydrazides. Synthesis, characterization, and cytotoxic effect. J Inorg Biochem 1994;54(3):221–33.
[20] Delley B. Hardness conserving semilocal pseudopotentials. Phys Rev B 2002;65:85403–9.
[21] Charmm JZ, Schaefer M, Tidor B, Venable RM, Woodcock HL, Wu X, et al. Modeling and Simulation Solutions for Chemicals and Materials Research, Accelrys Materials Studio (Version 5.0). San Diego, USA: Accelrys Software Inc.; 2009 <http://www.accelrys.com>.
[22] Hehre WJ, Radom L, Schlyer PVR, Pople JA. Ab Initio Molecular Orbital Theory. New York: Wiley; 1986.
[23] Kessi A, Delley B. Density functional crystal vs. cluster models as applied to zeolites. Int J Quantum Chem 1998;68:135–44.
[24] Hammer B, Hansen LB, Nørskov JK. Improved adsorption energetics within density-functional theory using revised Perdew-Burke-Ernzerhof functionals. Phys Rev B 1999;59:7413–21.
[25] Matveev A, Staufer M, Mayer M, Rösch N. Density functional study of small molecules and transition-metal carbonyls using revised PBE functionals. Int J Quantum Chem 1999;75:863–73.

[26] Zaky RR, Yousef TA. Spectral, magnetic, thermal, molecular modelling, ESR studies and antimicrobial activity of (E)-3-(2-(2-hydroxybenzylidene) hydrazinyl)-3-oxo-n(thiazole-2-yl)propanamide complexes. J Mol Struct 2011;1002:76–85.
[27] Yousef TA, Abu El-Reash GM, El Morshedy RM. Quantum chemical calculations, experimental investigations and DNA studies on (E)-2-((3-hydroxynaphthalen-2-yl)methylene)-N-(pyridin-2-yl)hydrazinecarbothioamide and its Mn(II), Ni(II), Cu(II), Zn(II) and Cd(II) complexes. J Polyhedron 2012;45:71–85.
[28] Garg BS, Kurup MRP, Jain SK, Bhoon YK. Manganese(II) complexes of substituted thio- and selenosemicarbazones of 2-acetylpyridine: Esr, magnetic and electronic spectral studies. Transit Met Chem 1988;13:92–5.
[29] Yousef TA, El-Reash GMA, Al-Jahdali M, El-Rakhawy ER. Synthesis, spectral characterization and biological evaluation of Mn(II), Co(II), Ni(II), Cu(II), Zn(II) and Cd(II) complexes with thiosemicarbazone ending by pyrazole and pyridyl rings. Spectrochim Acta A Mol Biomol Spectrosc 2014;129:163–72.
[30] Coats AW, Redfern JP. Kinetic parameters from thermogravimetric data. Nature 1964;20:68–9.
[31] Horowitz HH, Metzger G. A new analysis of thermogravimetric traces. Anal Chem 1963;25:1464–8.
[32] Broido A. A simple, sensitive graphical method of treating thermogravimetric analysis data. J Ploym Sci A 1969;2:1761–73.
[33] Britton HTS. Hydrogen Ions. 3rd ed. London: Chapman and Hall; 1942.
[34] Zaky RR, Yousef TA, Abdelghany AM. Computational studies of the first order kinetic reactions for mononuclear copper(II) complexes having a hard–soft NS donor ligand. Spectrochim Acta A Mol Biomol Spectrosc 2014;130:178–87.
[35] Silva FAM, Borges F, Guimarães C, Lima JLFC, Matos C, Reis S. Phenolic acids and derivatives: studies on the relationship among structure, radical scavenging activity, and physicochemical parameters. J Agric Food Chem 2000;48:2122–6.
[36] Siquet C, Paiva-Martins F, Lima JLFC, Reis S, Borges F. Antioxidant profile of dihydroxy- and trihydroxyphenolic acids – a structure–activity relationship study. Free Radic Res 2006;40:433–42.
[37] Miller NJ, Rice-Evans CA. Factors influencing the antioxidant activity determined by the ABTS•+ radical cation assay. Free Radic Res 1997;26:195–9.